GERMAN - MONGOLIAN INSTITUTE
FOR RESOURCES AND TECHNOLOGY

The present work was submitted to the Faculty of Engineering

Damage Simulation of Wind Turbine Tower and Effects on Modal Parameters

Bachelor Thesis

By

TUVSHINTUGS MUNKHBAT

Supervisor 1 / Examiner 1 **Professor Ph.D. Sungchil Lee**

Supervisor 2 / Examiner 2 **Professor Ph.D. Odbileg Norovrenchin**

Ulaanbaatar/Nalaikh, 05/16/2022

GERMAN - MONGOLIAN INSTITUTE
FOR RESOURCES AND TECHNOLOGY

Statutory Declaration

Munkhbat, Tuvshintugs	15348172644545
Last Name, First Name	Student ID Number

I hereby affirm in lieu of an oath that I provided the submitted bachelor thesis

xxx

I did not use any sources other than those stated. In case that the work is additionally submitted on a data medium, I declare that the written and the electronic form are completely identical. The work was not submitted in the same or similar form to any examination authority.

Place, Date	Signature

Abstract

Renewable energy is valued worldwide, natural resources are finite and CO2 emissions are accelerating global warming. The wind energy farm is seen as a viable renewable energy source in Mongolia since the country's unique topography makes wind energy feasible. Mongolia has various wind energy farms, which follow the global trend. The wind turbine tower, which is typically slender, is regularly subjected to high wind loads and is vulnerable to a variety of hazards. Because the breakdown of a wind turbine tower causes the entire turbine to collapse, it is critical to identify any expected tower damages and their impacts on structural soundness in advance so that the structure's owner can take measurements to prevent additional damage.

It is costly to do time scheduled maintenance all the time, and it will be too late when the structure fails. It is much more economically efficient to do condition-based maintenance, depending on the response of the modal parameters. Using these changes in wind turbine modal parameters, damage detection methods can be used to detect and estimate the severity of the damage inflicted upon the tower.

Firstly, damage simulation was introduced to the structure by lowering the Young’s modulus of targeted members of the structure. The effect of damage on modal parameters such as frequency and mode shapes of the tower was then investigated. Finally, frequency-based and mode shape-based damage detection methods were applied for damage localization.

Both damage localization algorithms accurately detected the inflicted damage, but frequency based damage detection method was only limited to finding one damage location. On the other hand, damage severity estimated by mode shape based damage detection was consistantly lower than the simulated damage severity.

Acknowledgement

I want to thank Prof. Sungchil Lee for his continuous support and always making time to help me when I struggled with my work. This Bachelor's thesis has proven to be a great hurdle to overcome, and every step to the finish line has been worth the time. Without his guidance and supervision, this would not have been possible.

I'd want to express my gratitude to all of GMIT's instructors and GMIT's students who generously contributed their vast knowledge and experience. This work is simply a collection of all the lessons I've learned during my time at GMIT.

Finally, I would like to express my deepest gratitude to my family and friends for their unconditional support and encouragement during my studies.

Contents

List of Figures

List of Tables

Abbreviation

HAWT	Horizontal Axis Wind Turbine
FBDD	Frequency Based Damage Detection
MBDD	Mode Shape Based Damage Detection
UAV	Unmanned Aerial Vehicle

Chapter 1 Introduction

1.1 Wind Energy sector in Mongolia

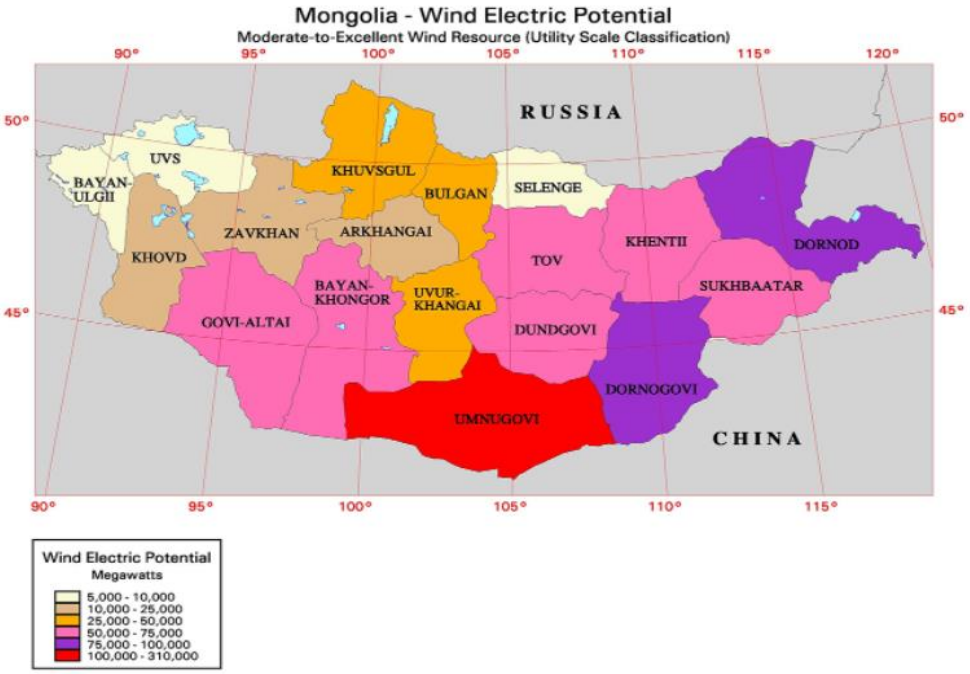

Figure 1: Mongolian Wind Energy Potential (1)

Mongolia offers a remarkable 1100 gigawatts(GW) wind energy potential, and if we include solar energy potential, it is estimated to be around 2600GW per year. Mongolia is also known as the “Land of the Eternal Blue Sky” and is sunny 260 days of the year. Which is suitable for solar panels around the country. In addition, we can see from Figure 1 that Mongolia has a tremendous amount of wind resources, particularly in the southern part of the country. The country is undergoing a major demographic shift, as people are gravitating towards the capital city Ulaanbaatar, where already 48% of the population resides in. This influx of people creates a demand for energy, and the demand is likely to increase every year.

Mongolia is currently going through significant issues providing adequate heat and energy for its people, particularly in the ger district. People in the ger districts don’t have access to basic heating, so they fire coal in stoves to survive the harsh winter times of Mongolia, which can drop well below -40°C. This excessive burning of coal during winter makes Ulaanbaatar one of the most air-polluted cities in the world, in a study of the 2018 world air quality report, Ulaanbaatar ranks as the fifth most polluted capital city on the planet(Figure 2). We can also

see that air pollution reaches the highest alarming levels in the winter months, from November to February. At this time, old coal power plants are the country's biggest producers of electricity and heat, with central networks.

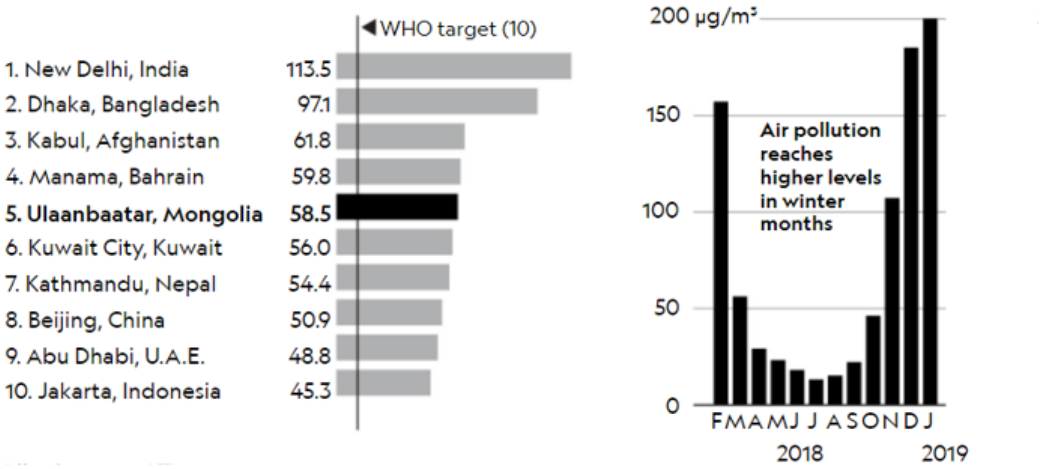

Figure 2:The most polluted capital in 2018, and monthly air pollution level in Ulaanbaatar (2)

Mongolia is rich in natural resources and have a thriving mining industry. In addition, Mongolia will see further mining developments, and demand for this expansion will grow stronger. Especially in the southern part of the country, where existing and future mining sites are likely to be located. Future power supplies are necessary for the industrial growth of this country. One of the solutions to combat all these obstacles is wind energy. Wind energy will prosper, as environmental factors suit the projects. Salkhit is the largest independent wind farm project now running in Mongolia, started supplying energy since the year of 2013.

1.2 Failures types in HAWT

Wind Energy is becoming a crucial part of our renewable energy supply and a solution for the energy crisis that is developing on a global scale. One of the remarkable examples is shown in Europe, where wind energy is the second-largest source of energy surpassing the usage of coal. The push towards renewable wind energy demands more up-to-date technology, with higher towers and higher efficiency.

Despite the significant advancements in turbine technology, the supporting structures still confront a number of hurdles, ranging from improving buckling and fatigue resistance to

adopting dependable mitigation mechanisms against the many risks posed by fire, earthquakes, and wind.

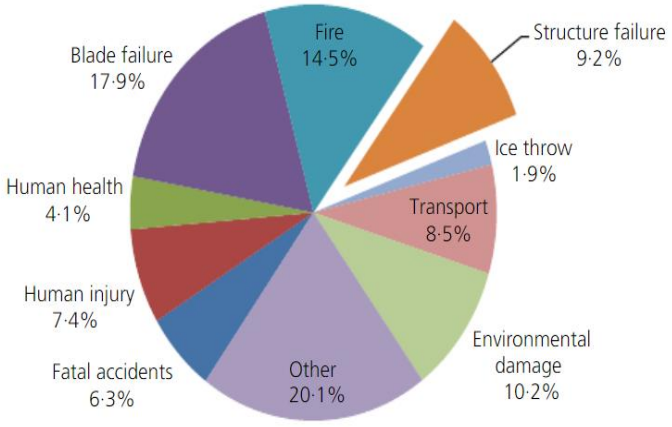

Figure 3 Failure type distribution of wind turbine incidents recorded between 1980 – 2016 (3)

Figure 3 shows the distribution of failure types for wind turbine incidents between 1980 and 2016. Following the information from (3), the most common factor for tower collapses are strong wind conditions, such as typhoons and hurricanes, since strong winds seem to be implicated in around 54.9% percent of the reports.

Fire hazard, wind turbine blade failure, bolt and fastener failure, or fatigue are all examples of second-level significance. Each of them has four cases in its database which have the same likelihood of recurrence, accounting for 5.6% percent of the total.

As Mongolia is a land-locked country, wind turbines in Mongolia will not experience typhoons and tropical cycles, whereas countries in the more East and Southeast Asia are more frequently affected. On the other hand, Mongolia will experience the same damage types that are more frequent in Europe and North America.

The failure rates of wind turbine components as a whole follow a bathtub curve that changes over time. Sometimes tower failure occurs in the early stages of life, sometimes known as infant failure. This usually refers to poor construction, material faults, and poor design. During normal operation, the failure rate is very consistent, and the structure poses the least risk over its lifetime.

The defective operation, inappropriate maintenance, and early material deterioration are all common reasons for failure within this time span. Near the end of the life span, the failure rate rises again, due to the wearing out of parts after a long period of operation as a result of poor maintenance or fatigue effects. Overall, at any stage in failure rate, the bathtub curve

appears to be affected by two primary factors. Which are extreme load circumstances, as well as human or mechanical flaws.

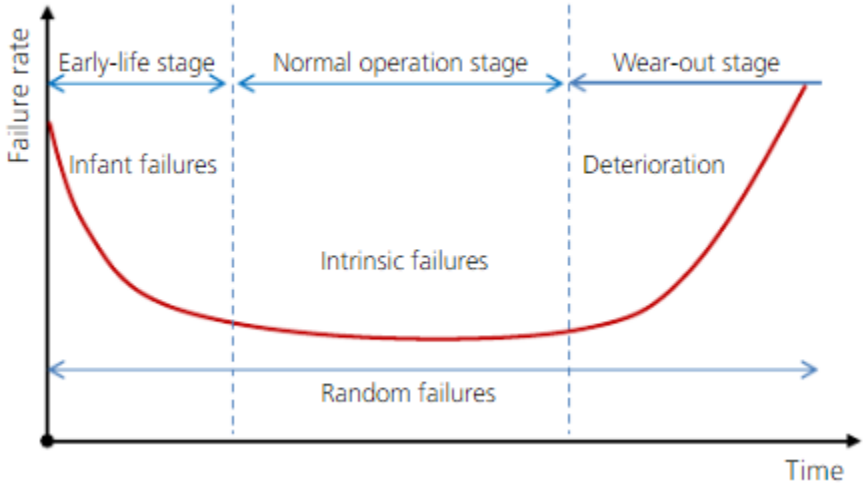

Figure 4:A Bathtub Curve for Failure Rate vs. Time (3)

The immediate repercussions include structural components exceeding their intended strength, which might result in chain effect. When a blade fails, for example, the load asymmetries rise, overburdening the tower section or causing windborne debris to collide with other structures. Human errors lead to improper construction, poor maintenance, and operation, all of which raise the risk level to unacceptable levels.

Bolt loosening generated by dynamic stresses is a common failure mechanism for the tower. Wind Turbine blades, on the other hand, are the structural elements most susceptible to damage. This is because of their greater complexity, unique materials, and exposure to high dynamic stresses. Static load-bearing parts including the tower structure, substructure, and foundations are thought to be less prone to deterioration. Among the many potential causes of its catastrophic collapse, the metallic tower's structure is vulnerable to all of the traditional dangers associated with thin-walled shells, such as buckling.

The support structure's major component is the tower. It can cost up to one-fourth of the entire cost, excluding foundation charges (Figure 5). The height of the tower is its most important feature. This is usually 1.5 times the rotor diameter; it is never less than 20 meters and can reach 150 meters or more (for 10–12 MW outputs).

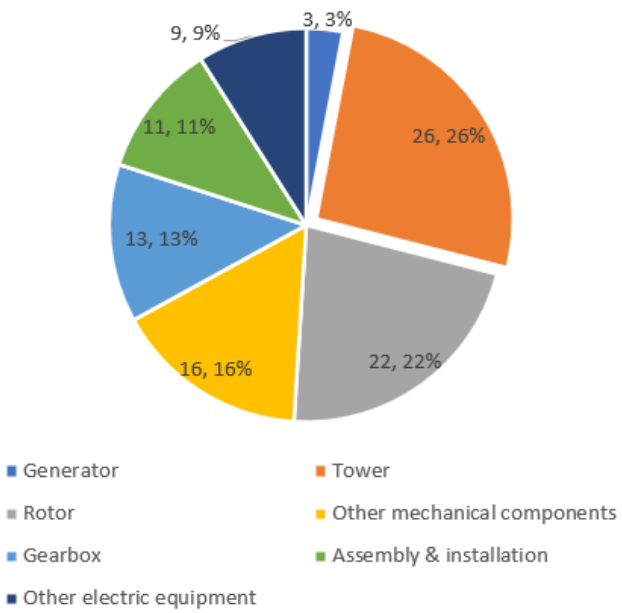

Figure 5: Estimated costs of a HAWT, as a percentage of the total and excluding foundations.Based on (4)

In terms of intensity and consistency, the higher the tower, the better the wind conditions. The tower might be tubular or latticed. Since the mid-1980s, this second design option has been more popular. The tower in this example is made up of thin-walled steel conical pieces with different diameters and wall thickness ratios. The survey teams can now gain access to the nacelle in a more practical and secure manner. The diameter of the tower, which is greatest at the base and smallest at the top, grows as the tower rises in height. Because of the possibility of coupled vibrations between the tower and the rotor, the stiffness of the tower is the most important parameter to consider in analyzing the global dynamics of Wind Turbines from a vibrational and structural health monitoring perspective.

1.3 Contribution of this research

Wind turbine towers are critical for supporting power-generating components including hubs, nacelles, and blades, as well as resisting wind stresses created by the blades. Damage occurrence in rotating parts is much more common than in the tower of the wind turbine. If a failure occurs in the tower, then the failure of the overall structure is guaranteed. Therefore, it is essential to secure the structural safety and stability of wind turbine towers, which may be damaged by unforeseen strong winds, through structural health monitoring and studying the effects on modal parameters of the tower.

In this study, the wind turbine model was made by Matlab, and damage was inflicted on various members of the structure. From the damaged and undamaged structure, a comparison was made, and numerical damage simulation effects on the modal parameters of the structure were observed. From the observation and the data we gathered, we can conclude if there is damage to the structure and using FBDD, MBDD, or other methods, we can localize the damage and predict the severity.

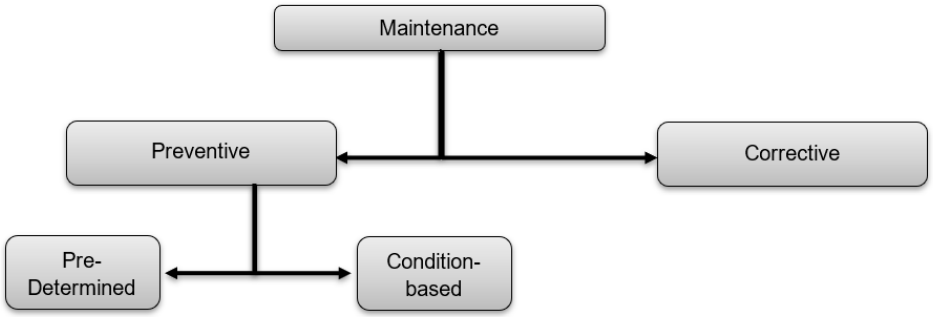

Figure 6: Breakdown of Maintenance

Predictive maintenance is important, as it predicts damages in its early stages. Corrective maintenance is undertaken after an obvious failure has been detected, with the goal of restoring a part or structure to a state where it can fulfill its intended purpose. It is both unplanned and unscheduled. As a result, corrective maintenance is frequently inevitable, with maintenance staff being forced to respond to equipment failure without notice and often without a complete understanding of the specific source of damage or failure. On the other hand, preventive maintenance tries to perform an inspection, replacement, or restoration before a component breaks in a pre-planned or predictable manner. This can assist reduce downtime while also boosting resource planning efficiency. Preventive maintenance is further separated into two types: scheduled (timed) and predictive (condition-based) shown in Figure 6.

Predictive maintenance compared to corrective and scheduled preventive maintenance is much more economically efficient and saves time, as cost versus a number of failures is shown in Figure 7, since there is no scheduled downtime. In the present climate, the wind industry is transitioning from scheduled planning to predictive (condition-based) monitoring, with the help of sensors, and continual monitoring systems being used to detect early warnings of irregularities on a global scale.

This is mostly accomplished by vibration-based signal analysis, SCADA data processing, and pattern recognition, all of which are accomplished using artificial intelligence methodologies (primarily machine learning and artificial neural networks). As previously said, all of these issues will be addressed in future, specialized works. On-site maintenance is still necessary for detailed, targeted examination once an abnormality is recognized or even localized. As a result, local nondestructive testing and global vibrational methods are not mutually exclusive. They, on the other hand, allow for quick and cost-effective maintenance planning. Based on a globally optimal exchange between prevention and repair costs, this concept is a crucial component of the "Intelligent Maintenance" paradigm.

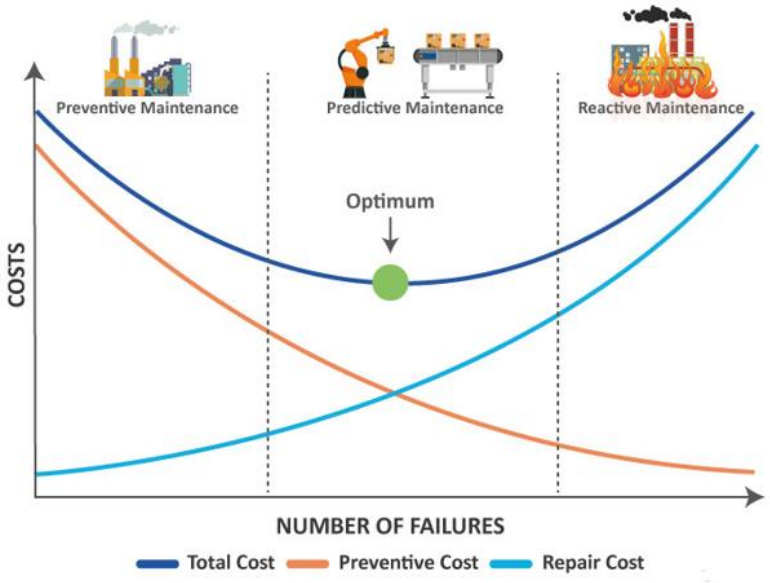

Figure 7: Total cost versus number of failures chart (5)

Chapter 2 Literature Review

2.1 Visual Inspection

The primary non-destructive testing methods for horizontal axis wind turbine integrity monitoring are explained and examined in this section. Please keep in mind that, while each strategy is described separately for clarity, they may and should be used together to compensate for each other's drawbacks.

For both the tower and the exterior of the nacelle, as well as the Wind Turbine blades, a simple visual inspection is still the most typical kind of maintenance assessment. This is usually done through binoculars from the bottom of the tower, or by roped maintenance employees and/or from a gantry or lift system during blade cleaning or inspection processes. These later options subject people to a certain level of risk and are not practical in adverse weather. Visual inspection of the mechanical components inside the nacelle is more problematic because of the limited area, but it is still possible with visual walkarounds. Borescope inspection or inspection pots in the gearbox can be used to conduct more extensive surveys.

The fundamental advantage of visual inspection is that it is essentially noninvasive because it is a contactless technique that does not modify the structural characteristics of the monitored system. However, it is obviously confined to only surface problems and defects. It takes a long time to examine the horizontal axis wind turbine because of its size. More importantly, it is a qualitative method; the accuracy of the evaluation results is greatly dependent on the skill of the inspectors and is limited by human errors. These evaluations are also difficult to compare between different maintenance crews.

There are two basic variables that can be used to categorize visual examination procedures. The first case is whether they require people on-site, and the second is whether they provide any form of assistance to human vision. The traditional visual examination is often carried out on-site by one or more technicians on a regular basis, without the use of artificial intelligence or advanced technology. It is also conceivable to have maintenance personnel use manned platforms in the first situation. Otherwise, people could be replaced by autonomous or non-autonomous robot platforms. These are necessary for tiny tubes and ducts, and they're also incredibly cost-effective when risk-adjusted inspections of components placed underwater or at perilous heights are required.

The second case is about whether or not to use computer vision techniques. Survey crews are frequently supplied with handheld gadgets, such as digital cameras. These, on the other hand, are frequently used for documentation rather than numerical data processing. These and other optical equipment can either improve or entirely replace human vision. The use of line or edge detection technologies, such as those used to identify surface cracks on wind

turbine blades, are two instances of the first situation. The term "automatic visual examination" is employed in this circumstance. Image or video-based approaches to automatic computer vision can be used.

These allow for the speedy and accurate assessment of vast surfaces, even for the tiniest surface imperfections, such as barely apparent impact damage caused by bird strikes on composite or steel materials. Unmanned aerial vehicles (UAVs) are the most popular alternative for robotized inspection. Other non-flying options are less popular, and practitioners and scholars have paid less attention to them.

2.2 Optical Methods

Image and video analysis are vast topics of study. Most optical measurement techniques are well-known and widely used; a good example is digital image correlation, which is well-known for experimental testing of materials in particular and is currently widely employed for full-field wind turbine strain inspection. Stereophotogrammetry can be utilized for strain measurements if numerous cameras are available. The technology has also been tried with photos captured by an unmanned aerial vehicle (UAV). With the exception of blade monitoring, direct image correlation measurements on the tower structure have been used less frequently.

Researchers are also interested in phase-based motion magnification, a more contemporary video processing technique for extracting modal parameters from subtle vibrations. This technology has been proved to be feasible for Structural Health Monitoring and has been used to wind turbine blades in conjunction with stereophotogrammetry. All of these solutions rely on the brightness amplitude and/or phase of the pixels in some way, and are thus restricted to the visible range of the electromagnetic spectrum. They are best employed off-site in controlled laboratory circumstances, but they have also been validated for on-site outdoor research with natural lighting.

Optical coherence tomography is another optical technology that was first introduced for non-direct cross-sectional scanning of biological tissues and then improved for higher depth resolution. The method relies on an exterior broad bandwidth source of light.

2.3 Mode Shape based Damage Detection Method

There are many ways to check for damage such as X-rays, optical methods, visual inspection, temperature measurements, and Infrared Thermography. Nevertheless, it is time-consuming and there are risks of staff workers getting into an accident for an overextended time being at heights.

With sensors placed throughout the wind turbine tower, we can have data to analyze the modal parameters of the structure. There are several studies showing ways to localize damage with changes in modal parameters. According to researchers (6) from their research, they came to the conclusion that mode shapes of a structure were much more sensitive to damage than change in natural frequencies.

In this study we have divided the tower to 16 sections along the line for simplification. From our modal parameter response we can have an investigation of mode shape based damage detection. In this section, we will attempt to find a methodology which localize damage and estimate the severity of damage wind turbine tower based on (7).

2.3.1 Damage Localization Theory

We are considering a vertical linear, undamaged structure with NE elements and N nodes. The i^{th} modal stiffness, K_i, of the arbitrary structure is given below.

$$K_i = \Phi_i^T C \Phi_i \tag{1}$$

Where i^{th} modal vector is Φ_i and the system stiffness matrix is *C*. K_{ij} is contribution of the j^{th} member to the i^{th} modal stiffness, where C_J is the j^{th} member contribution to the system stiffness matrix.

$$K_{ij} = \Phi_i^T C_J \Phi_i \tag{2}$$

For the i^{th} mode, the fraction of modal energy contained in the j^{th} member is (i.e., the sensitivity of the specific member to that specific mode) given by:

$$F_{ij} = K_{ij}/K_i \tag{3}$$

Assign an asterisk to the corresponding modal parameters in equations 1-3 that are associated with a later damage structure. Then for the damaged structure:

$$F_{ij}^* = \frac{K_{ij}^*}{K_i^*} = F_{ij}(1 + \sum_{k=1}^{NE} A_{ik}\alpha_k + H.O.T.) \tag{4}$$

Where K_{ij}^* and K_i^* are given by, respectively:

$$K_{ij}^* = \Phi_i^{*T} C_j^* \Phi_i^* \tag{5}$$

$$K_i^* = \Phi_i^{*T} C^* \Phi_i^* \tag{6}$$

Where A_{ik} denotes a set of coefficients related with the mode *i* and location *k;* α_k is the fraction of damage at location *k* in the structure; and H.O.T. denotes for higher order terms. When Equation 4 is divided by Equation 3, we obtain:

$$\frac{F_{ij}^*}{F_{ij}} = \frac{K_{ij}^*}{K_{ij}} \frac{K_i}{K_i^*} \tag{7}$$

The quantities C_J and C_j^* in Equations and 5 may be written as follows: Where the scalars E_j and E_j^*, respectively, are parameters representing the material stiffness properties of undamaged and damaged j^{th} member of the structure, and the matrix C_{jo} involves only geometric quantities like terms containing Poisson's ratio.

$$C_J = E_j C_{jo} \tag{8}$$

$$C_j^* = E_j^* C_{jo} \tag{9}$$

When we compare Equations 4 and 7, we notice the following observation: (1) We can write an equation for each mode for each location,(2) if the damage is to be specified in a small region, then we will have a larger number of equations to define the system; and and (3) we must find a way to determine the linear coefficients A_{ik} and higher order terms. This

complicates the calculation, so we need to figure out a technique to solve equation 7 without needing to figure out the solution of A_{ik}.

To respond to the question, we will use the following simplification. The geometry of mode shapes in the vicinity of an undamaged element of a structure changes very little when the structure is damaged elsewhere, according to experiment results. It also has been established experimentally that relative modal deformations (i.e., Φ_i) at a given location are larger after damage occurred (i.e., stiffness reduction occurs).

We simplify Equation 4 to the approximation that the modal strain energy F_{ij} in an element remains the same before and after the damaging process based on these observations and the assumption that the extent of damage in the structure is small. As a result, we propose the following simplification:

$$F_{ij} = F_{ij}^{*} \tag{10}$$

Equations 1, 2, 5, 6, 8, and 9 are substituted ino Equation 7, and by rearranging, we get:

$$\beta_{ij} = \frac{E_j}{E_j^{*}} = \frac{\left[\Phi_i^{*T}\, C_{jo}\, \Phi_i^{*}\right] K_i}{\left[\Phi_i^{T}\, C_{jo}\, \Phi_i\right] K_i^{*}} \tag{11}$$

The damage localization indication in which the term β_{ij} is the for the j^{th} member and i^{th} mode. If we set $K_i^{*} = \Phi_i^{*T} C \Phi_i^{*}$, all quantities on the right hand side (e.g., Φ_i and Φ_i^{*}) can be obtained or approximated from modal paramters derived from experimental measurements and the geometry C_{jo} of the structure.

It should be noted that using higher order approximations (e.g., Equation 4) to relate F_{ij} and F_{ij}^{*} results in more convoluted expressions, making it difficult to distinguish inflicted damage from measure modal quantities.

if β_{ij}>1, damage is detected at the j^{th} member and the i^{th} mode according to Equation 11. However, if the j^{th} member is at or near a node of i^{th} mode, the denominator of Equation becomes zero (i.e., F_{ij}<<1) resulting in a misleading damage prediction. This constraint (i.e., that of a false positive prediction) is handled in the following way, Because F_{ij}<<1 adding unity to both of Equation 10 yields:

$$1 = \frac{F_{ij}^* + 1}{F_{ij} + 1} \tag{12}$$

Equations 3 and 4 provide the following results when F_{ij}^* and F_{ij} are substituted:

$$1 = \frac{(K_{ij}^* + K_i^*)K_i}{(K_{ij} + K)_i K_i^*} \tag{13}$$

Utilizing expressions for K_{ij}^* and K_{ij} in Equations 2 and 5 along with the relationships given in Equations 8 and 9, Equation 13 is transformed to:

$$1 = \frac{E_j^*}{E_j} \frac{\left(\Phi_i^{*T} \mathrm{C}_{jo} \Phi_i^* + \frac{1}{E_j^*} \sum_{k=1}^{NE} \Phi_i^{*T} \mathrm{C}_k^* \Phi_i^*\right)}{\left(\Phi_i^T \mathrm{C}_{jo} \Phi_i + \frac{1}{E_j} \sum_{k=1}^{NE} \Phi_i^T \mathrm{C}_i \Phi_i\right)} \frac{K_i}{K_i^*} \tag{14}$$

From which a new β_{ji} may be defined as:

$$\beta_{ji} = \frac{\left(\Phi_i^{*T} \mathbf{C}_{jo} \Phi_i^* + \frac{1}{E_j^*} \sum_{k=1}^{NE} \Phi_i^{*T} C_k^* \Phi_i^*\right)}{\left(\Phi_i^T \mathbf{C}_{jo} \Phi_i + \frac{1}{E_j} \sum_{k=1}^{NE} \Phi_i^T \mathrm{C}_k \Phi_i\right)} \frac{K_i}{K_i^*} \tag{15}$$

On substituting Equations 8 and 9 into Equation 15, the damage localization indicator is simplified:

$$\beta_{ji} = \frac{\left(\Phi_i^{*T} \mathbf{C}_{jo} \Phi_i^* + \frac{1}{E_j^*} \sum_{k=1}^{NE} \Phi_i^{*T} E_k^* C_k^* \Phi_i^*\right)}{\left(\Phi_i^T \mathbf{C}_{jo} \Phi_i + \frac{1}{E_j} \sum_{k=1}^{NE} \Phi_i^T E_k \mathrm{C}_k \Phi_i\right)} \frac{K_i}{K_i^*} = \frac{\left(\Phi_i^{*T} \mathbf{C}_{jo} \Phi_i^* + \sum_{k=1}^{NE} \Phi_i^{*T} C_{ko}^* \Phi_i^*\right)}{\left(\Phi_i^T \mathbf{C}_{jo} \Phi_i + \sum_{k=1}^{NE} \Phi_i^T \mathrm{C}_{ko} \Phi_i\right)} \frac{K_i}{K_i^*} \tag{16}$$

The indicator β_{ji} has two significant components. The statement aims to characterize changes in stiffness at a specific point in terms of pre-damage and post-damage mode shapes, and the terms on the right hand side of Equation 16 can be measured or calculated from the structure's geometry. As a result, there are as many β_{ji} values as there are mode shapes for each damage location *j.*

We provide a single damage indicator for each location to account for all available modes(NM) in the damage localization scheme:

$$\beta_j = \frac{\sum_{i=1}^{NM} \left(\Phi_i^{*T} \mathbf{C}_{jo} \Phi_i^{\circ} + \sum_{k=1}^{NE} \Phi_i^{*T} C_{ko} \Phi_i^{\cdot}\right) K_i}{\sum_{i=1}^{NM} \left(\Phi_i^{T} C_{jo} \Phi_i + \sum_{k=1}^{NE} \Phi_i^{T} C_{ko} \Phi_i\right) K_i^{*}} \tag{17}$$

2.3.2 Classification criteria for damage localization

We then build more effective damage localization classification criteria. The locations of damage for a specific collection of modes are chosen based on a statistical rejection of hypothesis. To begin, each member's value β_j (*j*=1,2,3,….,*NE*) is treated as a realization of a random variable *β.* In other words, the collection of the damage indices, β_j , represents a sample population. For purposes of making a consistent comparison, location is classified into one of two groups. We first normalize the values of the indicator β_j (*j*=1,2,3,….,*NE*) according to the rule:

$$Z_j = \frac{\beta_j - \bar{\beta}}{\sigma_\beta} \tag{18}$$

The terms $\bar{\beta}$ and σ_β denote the mean and the standard deviation of the collection of β_j values, respectively.

The next step is to create an algorithm to sort the Z_{js} into damaged and undamaged categories. A solution to this problem can be found using a variety of techniques, including statistical hypothesis testing, signal detection and classification analysis, among others. We use a statistical pattern recognition technique and hypothesis testing to classify the damage pattern. The null hypothesis (i.e. H_o) is that there is no damage to the structure at the j^{th} location. The alternative hypothesis (i.e. H_1) is that j^{th} location of the structure is damaged. We select this decision rule as follows:

Choose H_1: when $Z_j \geq$ K
Choose H_0: when $Z_j <$ K

In which K is the number that reflects the level of significance of the test (e.g., if K=2, then the level of significance is 0.024)

2.3.3 Damage Severity Estimtaion Theory

Damage severity can be estimated directly from Equation 11. Let the fractional change in the stiffness of the j^{th} member be given by α_j, such that $\alpha_j \geq -1$, then by definition:

$$E_j^* = E_j(1 + \alpha_j)$$

$$\alpha_j = \frac{\left[\Phi_i^T C_{jo} \Phi_i\right]}{\left[\Phi_i^{*T} C_{j_0} \Phi_i^*\right]} \frac{K_i^*}{K_i} - 1$$

2.4 Frequency based Damage Detection Method

According to (6) their research, they came to the conclusion that mode shapes of a structure were much more sensitive to damage than change in natural frequencies. Natural frequencies are much easier to measure than mode shapes. However, for at least two reasons, the viability of exploiting frequency changes for damage localization is limited. First, severe damage can create very minor changes in natural frequencies, which can go unnoticed due to measurement or computational mistakes, especially in larger constructions. Variations in the structure's mass or measurement temperature may induce inaccuracies in the frequency changes detected. Then again(8), there are certain disadvantages using mode shapes. First, the damage is a local phenomenon that may have little impact on the lower mode forms that are typically observed in vibration studies of large structures. Second, external noises such as ambient loading or inconsistencies in sensor placements alter retrieved mode shapes. Finally, depending on how many sensors we use and the sensor coordinates are chosen may have a significant impact on the damage detection procedure's accuracy. In this section, damage localization from the perspective of frequency were formulated.

2.4.1 Damage localization theory

The damage sustained at predetermined sites can be anticipated using the corresponding sensitivity Eq.(1) for the multiple degree of freedom structural system with *NE* elements and *N* nodes:

$$\sum_{j=1}^{NE} F_{\mathrm{ij}}\alpha_{\mathrm{j}} = Z_{\mathrm{i}} \tag{1}$$

Where α_{j} (-1≤ α_{j} ≤0) is the damage caused at the j^{th} location, i.e., the fractional decrease in the stiffness parameter of the j^{th} element. If changes in mass are ignored, Z_{i} is the fractional shift in the i^{th} eigenvalue resulting to damage:

$$Z_{\mathrm{i}} = \frac{\delta\omega_{\mathrm{i}}^2}{\omega_{\mathrm{i}}^2} \tag{2}$$

In which $\delta\omega_{\mathrm{i}}^2$=$\omega_{\mathrm{i}}^{*2}$-$\omega_{\mathrm{i}}^2$. The term F_{ij} is the fraction of modal energy that is the sensitivity for the i^{th} mode that is centered in the j^{th} element it is calculated as follows:

$$F_{\mathrm{ij}} = \frac{\{\phi_{\mathrm{i}}\}^{\mathrm{T}}[C_{\mathrm{j}}]\{\phi_{\mathrm{i}}\}}{\{\phi_{\mathrm{i}}\}^{\mathrm{T}}[C]\{\phi_{\mathrm{i}}\}} \tag{3}$$

Where [C] is the system stiffness matrix, and $[C_{\mathrm{j}}]$ is the contribution of the j^{th} element to the system stiffness, and $\{\phi_{\mathrm{i}}\}$ is the i^{th} mode shape vector. Eq.(1) can be calculated to identify and size damage in the system once the quantity Z_{i} is has been experimentally measured and the sensitivity F_{ij} has been numerically computed. The inverse solution, on the other hand, is only conceivable if the number of damage variables is similar to the number of modes (i.e., *NE*≈*NM*). When *NE*>*NM*, the system could become inadequate, necessitating the use of alternative damage parameters estimation methods. In order to solve this challenge, an algorithm based on the frequency-change and sensitivity ratio described by (9) was proposed.

Imagine a structure system with *NE* elements (*j* =1,2,…,*q*,…,*NE*) and *NM* vibration modes (*i* =1,…,*m*,*n*,…,*NM*). For just about any two different modes *m* and *n* (*m* ≠ n), correspondingly, Eq. (1) is reformulated. When you divide Eq. (1) for mode *m* by the Eq. (1) for mode *n*, we recieve:

$$\frac{Z_{\mathrm{m}}}{Z_{\mathrm{n}}}=\frac{\sum_{j=1}^{NE} F_{\mathrm{mj}}\alpha_{\mathrm{j}}}{\sum_{j=1}^{NE} F_{\mathrm{nj}}\alpha_{\mathrm{j}}}=\frac{F_{\mathrm{m1}}\alpha_1+F_{\mathrm{m2}}\alpha_2+\cdots+F_{\mathrm{mq}}\alpha_{\mathrm{q}}+\cdots+F_{\mathrm{mNE}}\alpha_{\mathrm{NE}}}{F_{\mathrm{n1}}\alpha_1+F_{\mathrm{n2}}\alpha_2+\cdots+F_{\mathrm{nq}}\alpha_{\mathrm{q}}+\cdots+F_{\mathrm{nNE}}\alpha_{\mathrm{NE}}} \tag{4}$$

Eq(4) reduces to assumption that the structure is damaged at a single location *q*, such that $\alpha_{\mathrm{j}} \neq 0$ when $j = q$ but $\alpha_{\mathrm{j}} = 0$ when $j \neq q$:

$$\frac{Z_{\mathrm{m}}}{Z_{\mathrm{n}}}=\frac{F_{\mathrm{mq}}}{F_{\mathrm{nq}}} \tag{5}$$

The ratio of the fractional shift in the *m*th eigenvalue to the fractional shift in the *n*th eigenvalue is $Z_{\mathrm{m}}/Z_{\mathrm{n}}$. Also, $F_{\mathrm{mq}}/F_{\mathrm{nq}}$ is the sensitivity ratio for *m*th mode and *q*th element to the sensitivity of *n*th mode and *q*th element. As a result, Eq. (5), which equals the L.H.S to the R.H.S, defines the damage done at that region.

2.4.2 Classification criteria for damage localization

Equation (5) can be extended to include all measure *NM* modes.

$$Z_{\mathrm{m}}/\sum_{k=1}^{NM} Z_{\mathrm{k}}=F_{\mathrm{mq}}/\sum_{k=1}^{NM} F_{\mathrm{kq}} \tag{6}$$

We put an error index into Eq. (6), since it is only valid if element *q* is damaged:

$$e_{\mathrm{ij}}=Z_{\mathrm{m}}/\sum_{k=1}^{NM} Z_{\mathrm{k}}-F_{\mathrm{mq}}/\sum_{k=1}^{NM} F_{\mathrm{kq}} \tag{7}$$

Where e_{ij} denotes the i^{th} mode and the j^{th} location localization error, and $e_{\mathrm{ij}} = 0$ signifies that the damage is found at the j^{th} region using the i^{th} modal information. We form a new damage indicator (DI) for the j^{th} member to account for all available modes as follows:

$$DI_{\mathrm{j}}=\left[\sum_{i=1}^{NM} e_{\mathrm{ij}}^2\right]^{-\frac{1}{2}} \tag{8}$$

Where $0 \leq DI_{\mathrm{j}} \leq \infty$ and if DI_{j} approaches the local maximum point then the damage is located at element *j*

Chapter 3 Modeling of Wind Turbine Tower

3.1 Typical geometry of wind turbine tower in Mongolia

In this example, we will be using the Salkhit wind farm as our main target of structure in Mongolia. Salkhit is considered one of the first major wind farm projects in the country, it is located in Sergelen sum, Tuv aimag(75 kilometers from Ulaanbaatar). Started construction in 2011, and made the assembly in 2012, since june of 2013 it has been working non-stop. The wind turbine towers have been imported from GE wind energy which is a branch of GE Renewable Energy company. The investment for this project is around $122 million, the contribution of this has been proven to be fruitful, and it is estimated to reduce 190’000 tons of CO2 emission every year. The total output of this project will cover 5% of Mongolia’s total electricity needs.

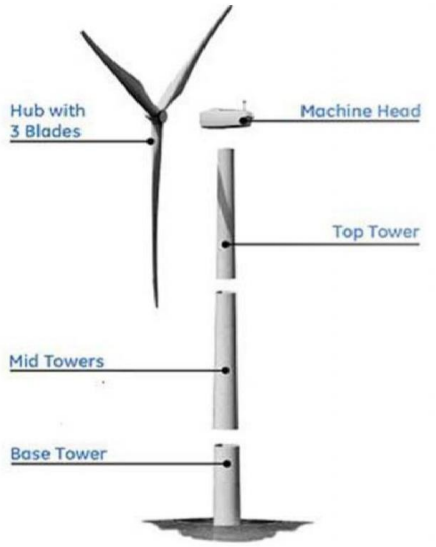

Figure 8: Breakdown of Salkhit Wind Turbine (10)

The demand for electricity in Ulaanbaatar grows larger every year, and this project helps by total capacity 49.6 megawatts. It is able to withstand the harsh weather conditions of Mongolia which can go down to -50°C during the winter and +40°C during summer times.

Figure 9: Salkhit wind farm (11)

The model of this wind turbine tower is GE 1.6-100, The wind turbine is mounted on top of a tubular tower. The tubular tower is manufactured in sections from steel plates. There are two types of GE1.6 100 wind turbine tower, first one is 80 meters tall and consists of three sections, the second one is 100 meters tall and consists of five different sections. In case of Salkhit farm, they use the 80-meter tall tower which consists of three different sections. Looking at the figure below, we can see the three sections divided into the top, mid, and base towers.

	Weight (kg)	Weight(lbs)	Length(m)	Length(ft-in)	Width (m) top/bottom	Width (ft-in) top/bottom
Top section 100m HH	25000	55100	22.4	73'6''	2.6/4.3	8'6''/14'1''
Mid section A 100m HH	36900	81400	21	68'11''	4.3/4.3	14'1''/14'1''
Mid section B 100m HH	48300	106500	21	68'11''	4.3/4.3	14'1''/14'1''
Mid section C 100m HH	56500	124600	18	59'1''	4.3/4.3	14'1''/14'1''
Bottom section 100m HH	60000	132300	15	49'3''	4.3/4.6	14'1''/15'1''
Top section 79.7m HH	32700	72100	29.5	96'9''	2.6/3.4	8'6''/11'2''
Mid section A 79.7m HH	46000	101500	26	85'4''	3.4/4.3	11'2''/14'1''
Bottom section 79.7m HH	62000	136700	22	72'2''	4.3/4.6	14'1''/15'1''

Table 1: Detail of the weight and dimensions of the wind turbine tower that is used in Salkhit wind farm

3.2 Description of Wind Turbine Tower

In this section, we will be simulating damage to the wind turbine tower by using Matlab. Damage is done by decreasing the Young's Modulus of certain members in the structure. The test structure selected here is a wind turbine tower that is divided into 16 different members along the tower. All members have uniform steel section of 20mm in thickness and 2m in diameter shown in Figure 10. Values of the material and geometric properties are as follows: the mass density, ρ=7800kg/m^3; the elastic modulus, E=210'000N/mm^2; Poisson's ratio, v=0.3; the cross-sectional area, A=0.124m^2; the second moment of inertia, I=0.06mm^4. The displacement of nodes of mode shapes will be only in the 'x' axis, this simulation will be limited to only one degree of freedom, in each node there will be translational and rotatioanal displacement in the 'x' axis. Nonetheless the translational displacement will be given more consideration and of importance.

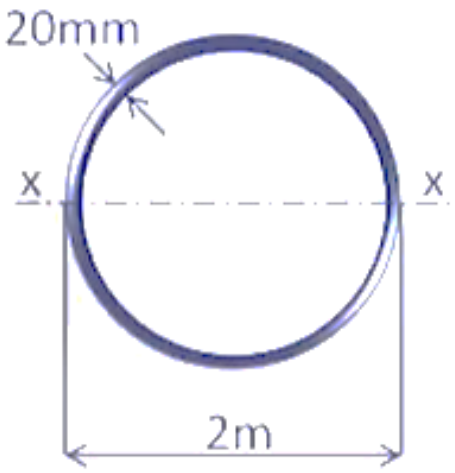

Figure 10.1 Schematic of the wind turbine tower from the X axis

Firstly, the undamaged wind turbine tower modal properties response and mode shapes must be calculated and demonstrated. Numerically generated frequencies and mode shapes for the first 5 modes of undamaged structure are shown below in Figure 11.

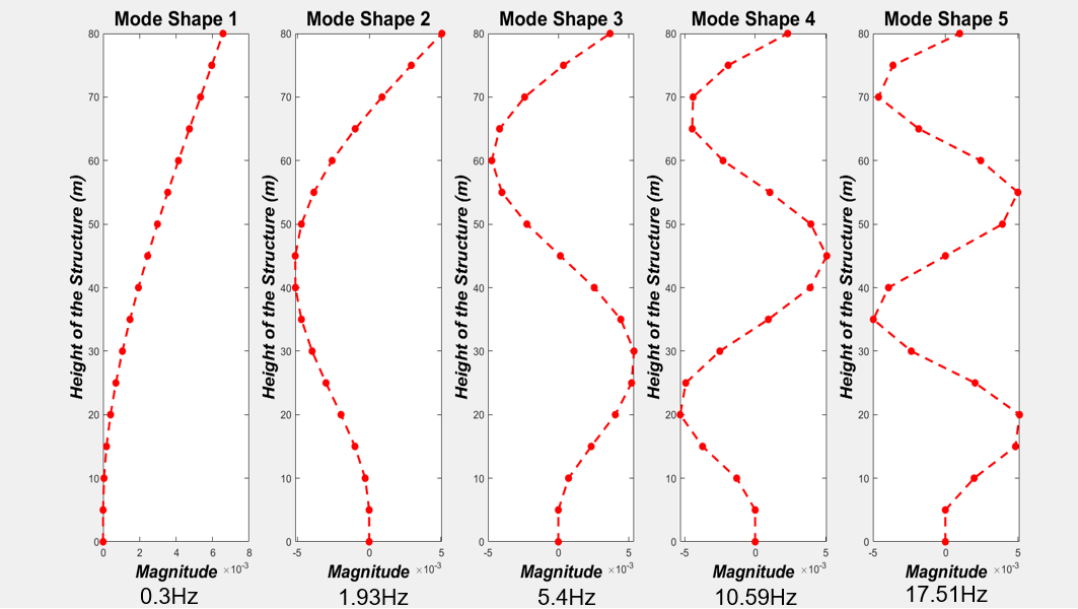

Figure 11: Mode shapes for the first 5 modes of undamaged structure

3.3 Damage effect on Modal Parameters

Case	Member(s)	Damage	Case	Member(s)	Damage
1	**4**	**-50%**	**4**	**12**	**-10%**
2	**8**	**-50%**	**5**	**5,11**	**-50%**
3	**12**	**-50%**	**6**	**7,13**	**-50%**

Table 2: Six damage scenarios

Six damage cases were evaluated in this study (as shown in Table 2). Damage to the structure was simulated in all situations by lowering the elastic modulus of the corresponding members. The 8 damage locations were simulated in the 6 damage scenarios, with the first four damage cases limiting the damage to a single spot on the test structure.

Note that Cases 3 and 4 are focused on Member 12, with two different damage magnitudes simulated. The test structure were damaged in two places in cases 5 and 6. Since the damage detection method used here ignores damping, damping coefficients were not determined in this study. Damage scenario 4 will be considered the least severe damage in

the structure representing the smallest change, and damage scenario 5 and 6 are considered the most severe, because damage is done in multiple members of the tower.

3.3.1 Effect on Natural Frequency

Mode Number	Damage Case						Undamaged Case
	1	2	3	4	5	6	
1	0.29Hz	0.3 Hz	0.3 Hz	0.31 Hz	0.29 Hz	0.3 Hz	0.3 Hz
2	1.93 Hz	1.83 Hz	1.87 Hz	1.92 Hz	1.84 Hz	1.83 Hz	1.93 Hz
3	5.27 Hz	5.38 Hz	5.07 Hz	5.36 Hz	4.91 Hz	5 Hz	5.4 Hz
4	10.14 Hz	10.12 Hz	10.28 Hz	10.54 Hz	10.28 Hz	9.9 Hz	10.59 Hz
5	17.11 Hz	17.3 Hz	17.44 Hz	17.51 Hz	16.89 Hz	16.23 Hz	17.51 Hz

Table 3: Post-damage frequencies of test structure

The frequency of the post-damage cases from one to six are compared to the undamaged frequency of the tower in Table 3, and the first five modes of the mode shapes were calculated. Damage case 4 and undamaged case frequencies are almost identical, since the damage on case 4 is considered really low compared to other cases. Damage Case 5 and 6 which has two damaged members are considered most severe in the system, and the most severe case frequencies compared to the undamaged frequencies are much lower compared to other damaged cases. During operational modal analysis, with readings from the sensors, particular SCADA system can calculate the frequencies of mode shapes with repetitive interval of time. From this observation, we could come to a conclusion that if the frequencies of the mode shapes get lower, there might be a damage in the system.

Damage cases 1, 2, and 3 were limited to only a single location in the system, and they are members 4, 8, and 12 respetively. Member 4 of the tower is the nearest member to the base of the tower, and member 12 is the furthest one away from the base of the structure. In the first three modes of damage cases 1 to 3, as the member is located further away from the base of the structure, the frequencies of mode shapes gets lower. Eventhough they are inflicted the same magnitude of damage.

3.3.2 Effect on Mode Shapes

The frequencies and mode shapes of the first 5 modes of undamaged structure and Damage Case 2 are listed respectively, in Table 4 and Table 5 below. Eventhough the frequencies of the of the damaged and undamaged structures are close, but the modal amplitudes are very different from each other.

Member	Mode 1 (0.3Hz)	Mode 2 (1.93Hz)	Mode 3 (5.4Hz)	Mode 4 (10.59Hz)	Mode 5 (17.51Hz)
	X-dir	X-dir	X-dir	X-dir	X-dir
1	8.16E-13	-1.78E-11	8.16E-11	-2.24E-10	4.77E-10
2	4.80E-05	-0.00028	0.000725	-0.00131	0.001986
3	0.000186	-0.00099	0.00234	-0.00374	0.004845
4	0.000406	-0.00196	0.004053	-0.00532	0.005123
5	0.000699	-0.003	0.00521	-0.00493	0.002052
6	0.001058	-0.00396	0.005383	-0.00251	-0.00235
7	0.001473	-0.0047	0.004442	0.000938	-0.00497
8	0.001936	-0.00512	0.002555	0.003909	-0.00392
9	0.002441	-0.00513	0.000142	0.005086	6.01E-06
10	0.002979	-0.00471	-0.00224	0.003953	0.003942
11	0.003544	-0.00384	-0.00401	0.001047	0.005009
12	0.004129	-0.00258	-0.00473	-0.00228	0.002442
13	0.004729	-0.00097	-0.00418	-0.00447	-0.00184
14	0.005339	0.000893	-0.00239	-0.00441	-0.00462
15	0.005954	0.002925	0.00036	-0.00192	-0.00362
16	0.006571	0.005044	0.003679	0.002307	0.000988

Table 4: Modal amplitudes for Undamaged Case

Member	Mode 1 (0.3Hz)	Mode 2 (1.83Hz)	Mode 3 (5.38Hz)	Mode 4 (10.12Hz)	Mode 5 (17.3Hz)
	X-dir	X-dir	X-dir	X-dir	X-dir
1	7.83E-13	-1.62E-11	7.91E-11	-2.17E-10	4.37E-10
2	4.62E-05	-0.00027	0.000705	-0.0013	0.001834
3	0.000179	-0.00096	0.00228	-0.00374	0.004493
4	0.000392	-0.0019	0.003955	-0.00542	0.004793
5	0.000675	-0.00295	0.005096	-0.00516	0.001985
6	0.00102	-0.00394	0.005291	-0.00283	-0.00214
7	0.001421	-0.00476	0.004412	0.000733	-0.00472
8	0.001868	-0.0053	0.002627	0.004137	-0.00405
9	0.002374	-0.00531	0.000186	0.005298	2.36E-05

10	0.00293	-0.00475	-0.00226	0.003663	0.004173
11	0.003512	-0.0038	-0.00407	0.000683	0.005187
12	0.004113	-0.00251	-0.0048	-0.00243	0.002427
13	0.004728	-0.00092	-0.00423	-0.00432	-0.00204
14	0.005353	0.000902	-0.00241	-0.00409	-0.00487
15	0.005984	0.002866	0.000384	-0.00166	-0.00376
16	0.006617	0.004907	0.003756	0.002306	0.001072

Table 5: Modal Amplitudes for Damage Case

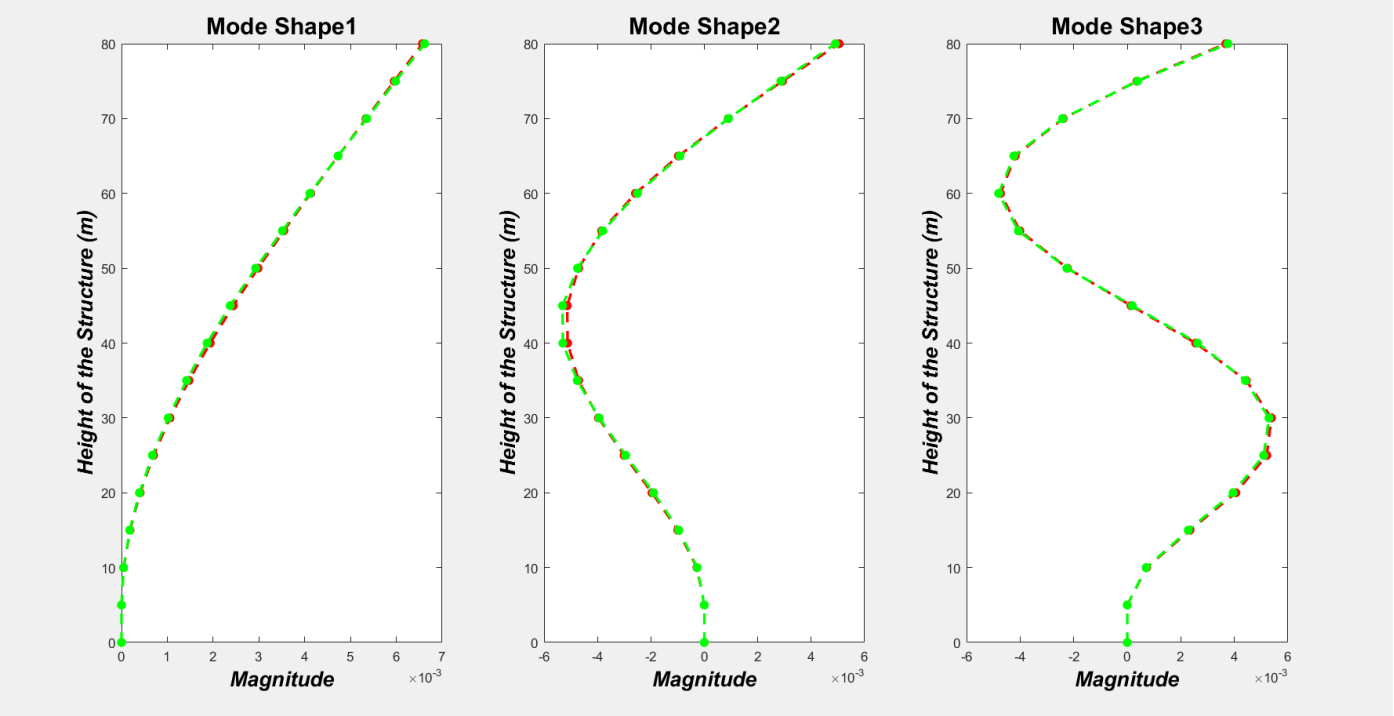

Figure 12: Mode shape and modal displacement difference between undamaged structure and Damage case 2 (red-undamaged, green-damaged)

Observing the figure above, in the first mode shape of Figure 12, there is slight divergence between the curves. Especially between the height of 35m and 50m, and the rest are almost in sync. In the second mode shape, there is slight divergence between the height of 40m and 50m. In the third mode shape, it is between 20m and 30m. The actual damage is done on the 8th member of the structure, which is located at the 40m height of the structure. Just from observing this graph, it is difficult to precisely locate the damaged member of the structure. This is the reason why we should have a damage detection algorithm, which we will explore more on the next section.

Chapter 4 Damage Localization

4.1 Damage localization by MBDD method

Over all damage prediction process will be using the following four steps: Firstly, we identified modal parameters of the test structure(undamaged), secondly we introduced damage to our structure by six different damage cases, thirdly we selected a damage detection model of the test structure, and finally, we located damage and estimated the severity of damage in the test structure. Here, by damage detection model, we mean a mathetical model of a structure with one translational and rotational degree of freedom corresponding as imitation of sensor readings.

In damage localization and severity estimation, firstly we were tasked to develop a damage localization indicator equation, which we have formulated (Equation 17) in the previous section. Secondly we established a criteria to know which members are damaged or undamaged. We established level of significance to be K=2, If Z_j>2 then there is significant damage in the member, and if Z_j<2 then there is no significant damage in the member. Thirdly, latter criteria was used to plot potential damage in the structure. Potential damage locations for the 6 damage cases were plotted below. Finally we have estimated the severity of the damage using Equation 21. The comparison between simulated damage and predicted damage severity estimation are listed in Table 6.

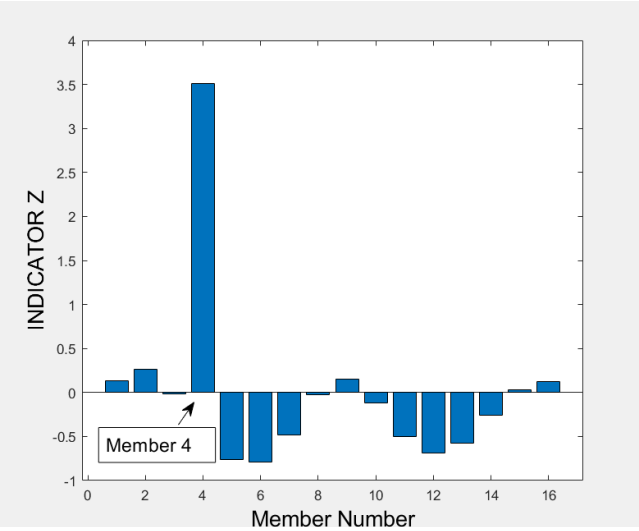

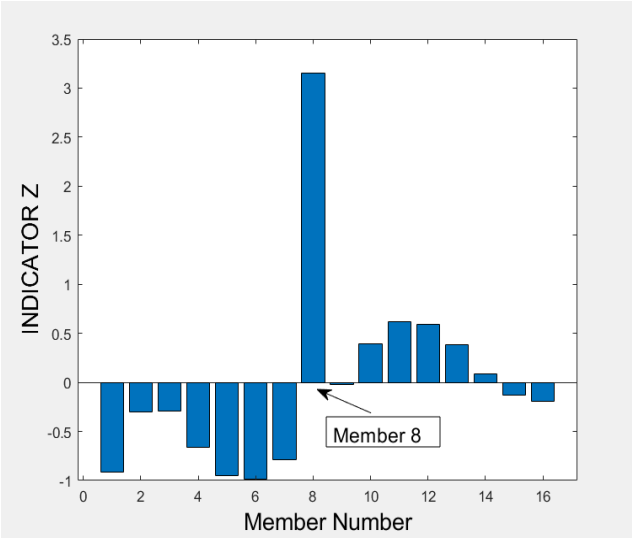

Figure 13a: Damage case 1

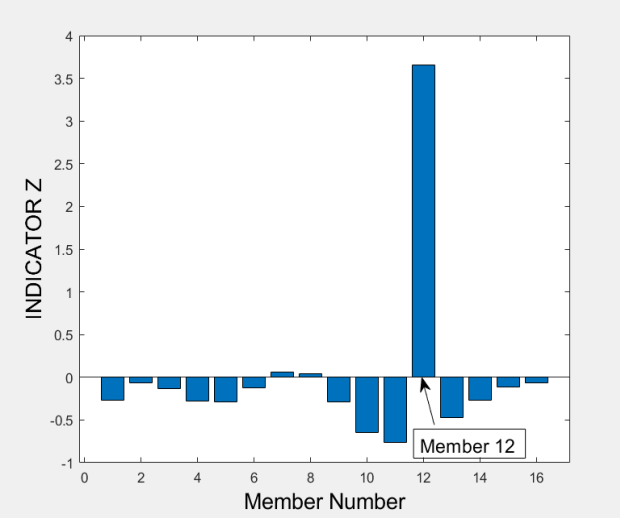
INDICATOR Z
Member Number
Member 12

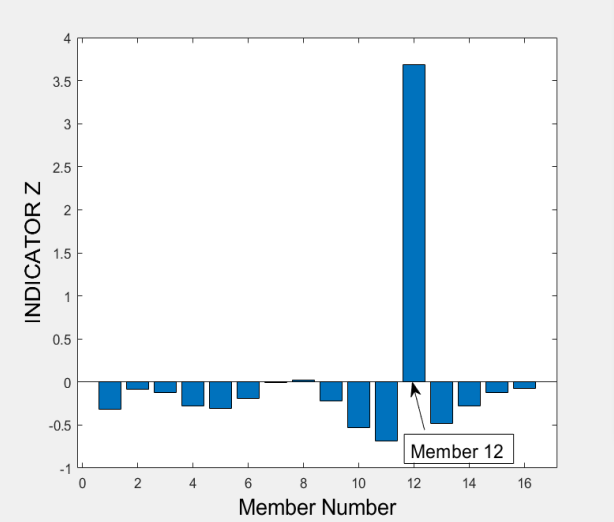
INDICATOR Z
Member Number
Member 12

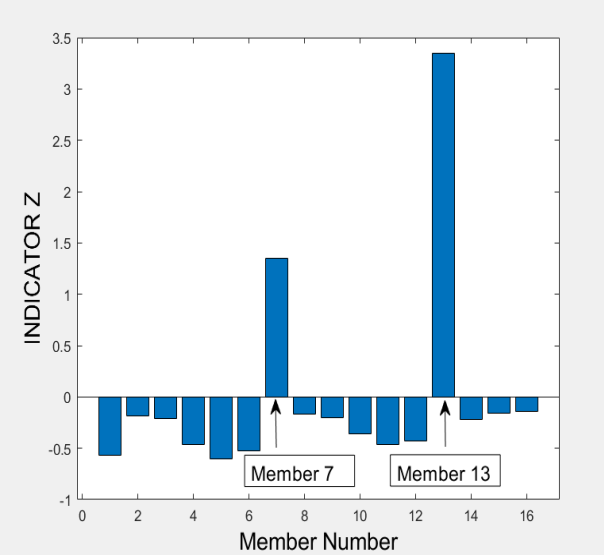
INDICATOR Z
Member Number
Member 7
Member 13

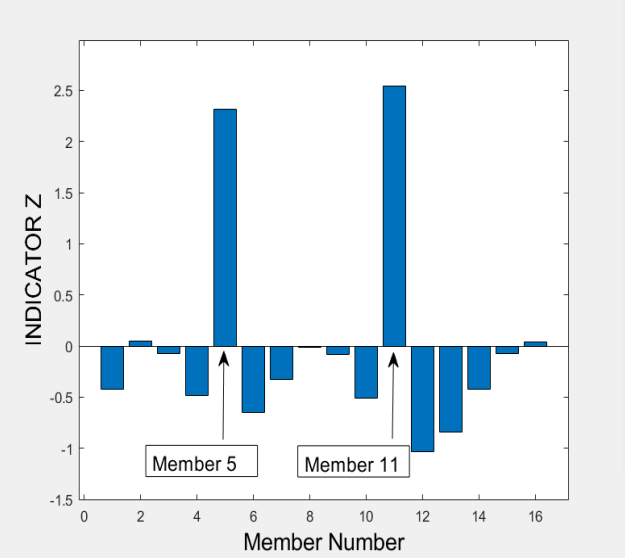
INDICATOR Z
Member Number
Member 5
Member 11

4.2 Damage severity estimation by MBDD method

Damage Case	Damage Locations	Simulated Magnitudes	Predicted Magnitudes	Simulated Predicted Ratio
1	4	-0.5	-0.19	0.38
2	8	-0.5	-0.2	0.4
3	12	-0.5	-0.2	0.4
4	12	-0.1	-0.03	0.3
5	5, 11	-0.5, -0.5	-0.18, -0.19	0.36, 0.38
6	7, 13	-0.5, -0.5	-0.18, -0.16	0.36, 0.32

Table 6: Severity estimation results in the test structure

After viewing the damage localization and severity estimation, following observations are made. Firsty, all of the damage localization predictions made in 6 damage cases are accurately predicted except for Damage case 5, which had two members introduced to damage(members 7 and 13).

Member 13 damage significance is Z_j>2, and member 7 damage significance is Z_j<2. Nonetheless observing Figure 13e, we can obviously conclude that member 7 and member 13 are damaged. If we lower the significance level K=2 to K=1, all of the damage cases are accurately localized. Secondly, no inaccurate predictions were made, for example additional locations which were not given simulated damage. Thirdly, in the severity prediction, it is underestimating our severity by a factor of 0.36 in average.

4.3 Damage localization by FBDD method

Case	Members	Damage	Case	Member	Damage
1	3	-10%	4	12	-10%
2	6	-10%	5	15	-10%
3	9	-10%	6	4,8	-10%

Table 7: Damage Cases for FBDD method

In frequency based damage detection, the needed modal parameters are undamaged and post-damage natural frequencies and undamaged structures mode shapes. In damage localization by Frequency Based damage detection, 6 new damage cases were made, in Table 7 above. From damage case 1 to 5, damage was inflicted only one member of the

structure, and damage case 6 was made on two members of the structure by lowering the stiffness of the material by 10%.

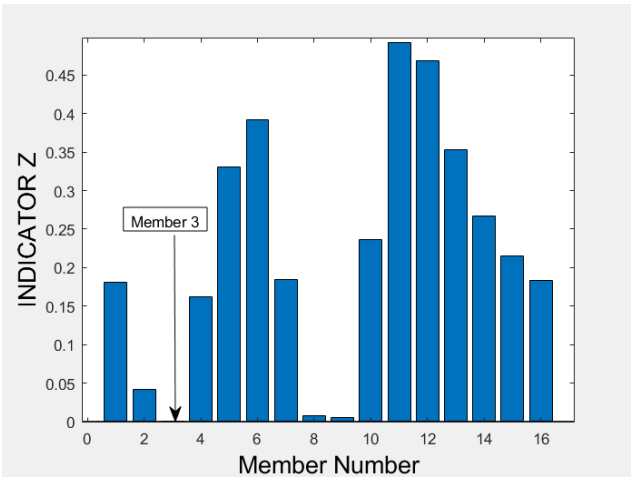

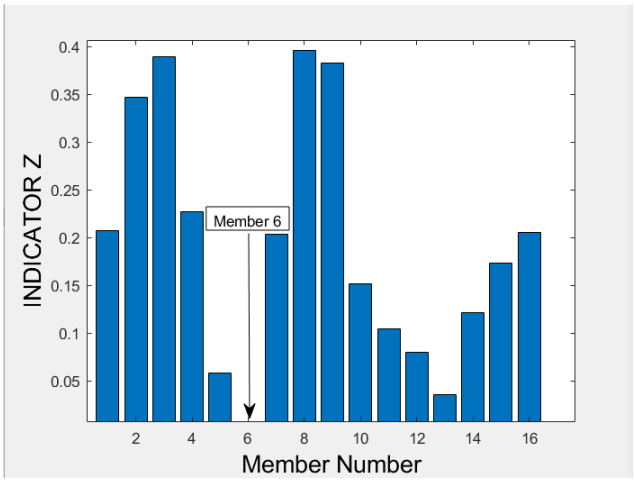

Figure 14a: Damage case 1

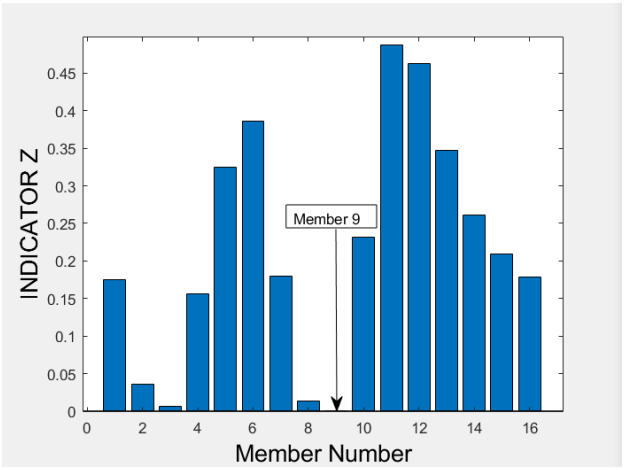

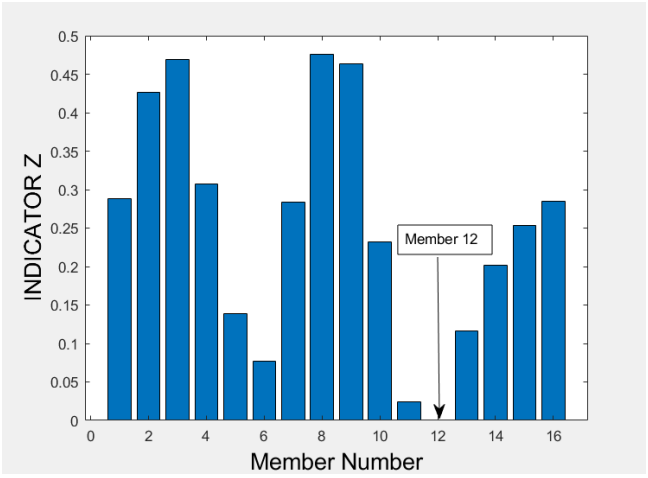

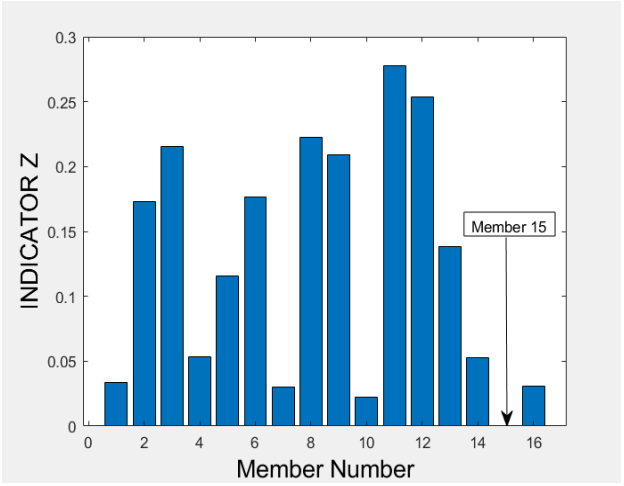

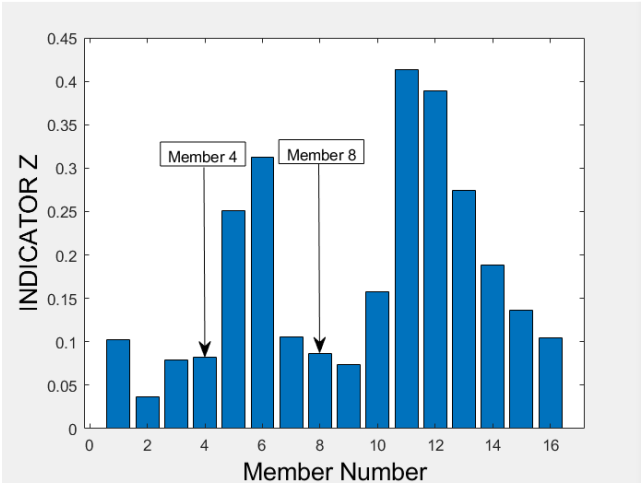

The ratio of the fractional shift in the *m*th eigenvalue to the fractional shift in the *n*th eigenvalue is $Z_{\mathrm{m}}/Z_{\mathrm{n}}$. Also, $F_{\mathrm{mq}}/F_{\mathrm{nq}}$ is the sensitivity ratio for *m*th mode and *q*th element to the sensitivity of *n*th mode and *q*th element. Calling back to equation 7,

$$e_{\mathrm{ij}} = Z_{\mathrm{m}}/\sum_{k=1}^{NM} Z_{\mathrm{k}} - F_{\mathrm{mq}}/\sum_{k=1}^{NM} F_{\mathrm{kq}} \tag{7}$$

Where e_{ij} denotes the i^{th} mode and the j^{th} location localization error, and e_{ij} = 0 signifies that the damage is found at the j^{th} region. From damage cases 1 to 5, which are only damaged at one location of the structure are correctly localized. FBDD seems to have its limitations, for example, in case of damage case 6 where two members are inflicted damages. The graph suggest that there are no damage detected in the structure, when in fact, it is severely weakened in two locations of the structure.

Eq.(1) can be calculated to identify damage in the system once the quantity Z_{i} is has been experimentally measured and the sensitivity F_{ij} has been numerically computed. The inverse solution, on the other hand, is only conceivable if the number of damage variables is similar to the number of modes (i.e., *NE*≈*NM*). The current state of the test structure is *NE*>*NM*, the system could have became inadequate, it was necessary to use the alternative damage parameters estimation methods. In order to solve this challenge, an algorithm based on the frequency-change and sensitivity ratio described by (9) was used, and from observation, it accurately localized damage when there is only damage on one member of the structure.

Chapter 5: Conclusion

This research was aimed to study the effects of modal parameters of the wind turbine tower when damage was introduced. After defining a simplified version of wind turbine tower in matlab, simulation of damage was given to varied members of the structure by lowering the Young's modulus.

From observing the frequency and the mode shapes of post-damage cases, the following conclusions were made. Firstly, the natural frequencies of the modes were relatively lower compared to the pre-damage structure's natural frequencies. If the frequencies of the modes are lower, there can be an assumption that there might be damage in the system. Secondly, comparing the structure's post-damage and pre-damage modal amplitudes in Figure 12, significant divergence in the graph can be an indication of damage.

Two damage localization methods were used, FBDD and MBDD. Firstly in MBDD, the algorithm accurately localized damage in the structure, even when there are multiple damaged locations in the structure. The significance level was initially chosen to be K=2, but from the results, it is safe to lower the significance level to K=1 and it would still accurately localize the damage. In severity estimation, the result consistently underestimated the inflicted damage by a factor of 0.36, this is related to equation 10. Where approximation $F_{ij} = F_{ij}^{*}$ that the modal strain energy in an element remains the same before and after the damaging process. Secondly in FBDD, the algorithm accurately localized the damage only if there was one damaged location in the structure, if there were more than one damaged location, then false predictions were made. No severity estimation was made, and it is only limited to localizing one damaged location in the structure.

Although these findings are encouraging, but keep some limitations in mind. Only two degree of freedom was used in this study, which were the translational and rotational displacement in the "x" axis. Real wind turbine tower is much more complex in nature.

References

1. http://www.cleanenergy.mn/en/mongol-salhi/page.
2. https://www.nationalgeographic.com/environment/article/mongolia-air-pollution.
3. Ma Y, Martinez-Vazquez P, Baniotopoulos C. Wind turbine tower collapse cases: a historical overview. Proceedings of the Institution of Civil Engineers - Structures and Buildings. 2019 Aug;172(8):547–55.
4. Ribrant J, Bertling LM. Survey of Failures in Wind Power Systems With Focus on Swedish Wind Power Plants During 1997–2005. IEEE Transactions on Energy Conversion. 2007 Mar;22(1):167–73.
5. https://www.assetinfinity.com/blog/reactive-vs-preventive-vs-predictive.
6. Rubin S, Coppolino RN. Flexibility Monitoring of Offshore Jacket Platforms. In: All Days. OTC; 1983.
7. Kim J, Polar NSIJ of O and, 1995 undefined. Damage detection in offshore jacket structures from limited modal information. onepetro.org [Internet]. 1995 [cited 2022 May 9];5. Available from: https://onepetro.org/IJOPE/article-abstract/26815/Damage-Detection-In-Offshore-Jacket-Structures
8. Kim JT, Ryu YS, Cho HM, Stubbs N. Damage identification in beam-type structures: frequency-based method vs mode-shape-based method. Engineering Structures. 2003 Jan;25(1):57–67.
9. KIM JT, STUBBS N. IMPROVED DAMAGE IDENTIFICATION METHOD BASED ON MODAL INFORMATION. Journal of Sound and Vibration. 2002 Apr;252(2):223–38.
10. https://www.yumpu.com/en/document/view/14055969/appendix-a-turbine-manufacturer-technical-specification-16mw.
11. https://inhabitat.com/the-salkhit-wind-farm-is-mongolias-first-major-wind-power-project/.

Appendix

Mode shape based damage detection

```
clc
clear all

nelm=16;
ndof= 2*nelm+2 ;
M(ndof,ndof)=0.0;
K(ndof,ndof)=0.0;

roh=7800;
A=0.124;
E=2E11; %(N/mm^2)
 I=0.06; %(mm^4)
 l=80/nelm;
 Ke(1,1)= (E*I/l^3)*12;
 Ke(1,2)= (E*I/l^3)*6*l;
 Ke(1,3)= (E*I/l^3)*(-12);
 Ke(1,4)= (E*I/l^3)*6*l;
 Ke(2,2)= (E*I/l^3)*4*l^2;
 Ke(2,3)= (E*I/l^3)*(-6*l);
 Ke(2,4)= (E*I/l^3)*(2*l^2);
 Ke(3,3)= (E*I/l^3)*12;
 Ke(3,4)= (E*I/l^3)*(-6*l);
 Ke(4,4)= (E*I/l^3)*(4*l^2);
 Me= (roh*A*l/420)*[156 22*l 54 -13*l; 22*l 4*l^2 13*l -
3*l^2; 54 13*l 156 -22*l; -13*l -3*l^2 -22*l 4*l^2] ;
 for i=1:4
     for j=1:4
         Ke(j,i)= Ke(i,j);
     end
 end
 p=0;
 q=0;
 for ne=1:nelm
    for ii=1:4
        for jj=1:4
            M(p+ii,q+jj)=M(p+ii,q+jj)+ Me(ii,jj);
            K(p+ii,q+jj)=K(p+ii,q+jj)+ Ke(ii,jj);
         end
    end
    p=p+2;
```

```
    q=q+2;
 end

    K(1,1)=1E15;
    K(2,2)=1E15;
%*******************************
% ei=eig(K,M);
[evec,eval]=eig(K,M);


for i=1:ndof;
    eval(i,i)=sqrt(eval(i,i));
    fhz(i,i)= eval(i,i)/(2*pi);
end
%Consider only Vertical DOF

for i=1:nelm
    k1=i*2-1;
   V(i,1)=evec(k1,1);
   V(i,2)=evec(k1,2);
   V(i,3)=evec(k1,3);
   V(i,4)=evec(k1,4);
   V(i,5)=evec(k1,5);

end



%*********************************************************
%The ith modal stiffness, Ki of the arbitrary structure
Ki(1,ndof)=0;
for i=1:ndof
    Ki(1,i)=evec(:,i)'* K * evec(:,i);
end

%*********************************************************
%Defining Kj the contribution of the jth member to the
system stiffness
%matrix
Kj(ndof,ndof,nelm)=0.0;
a=0;
 b=0;
 for ne=1:nelm
```

```
    for ii=1:4
        for jj=1:4
            Kj(a+ii,b+jj,ne)=Kj(a+ii,b+jj,ne)+
Ke(ii,jj);
         end
    end
    a=a+2;
    b=b+2;
 end
Kj(1,1,1)=1E15;
  Kj(2,2,1)=1E15;

%*******************************************************
%The contribution of the jth member to the ith modal
stiffness Kij
Kij(nelm,ndof)=0.0;
for i=1:nelm
    for j=1:ndof
    Kij(i,j)=evec(:,j)'* Kj(:,:,i) * evec(:,j);
    end
end


%*******************************************************
%Defining Young's Modulus (Ej) of the system, and
solving Kjo involving the
%geometric quantities of the system


Kjo(ndof,ndof,nelm)=0.0;
a=0;
  b=0;
for ne=1:nelm
    for ii=1:4
        for jj=1:4
           Kjo(a+ii,b+jj,ne)=Kj(a+ii,b+jj,ne)/E;
        end
    end
    a=a+2;
    b=b+2;
end

%DAMAGED scenorio of the system
Kdam(ndof,ndof)=0.0;
```

```
p=0;
   q=0;
D=12;
 for ne=1:nelm
     if ne == D
       for ii=1:4
        for jj=1:4
          Kdam(p+ii,q+jj)=Kdam(p+ii,q+jj)+
Ke(ii,jj)*0.9;
        end
       end
      else
    for ii=1:4
        for jj=1:4
           Kdam(p+ii,q+jj)=Kdam(p+ii,q+jj)+ Ke(ii,jj);
         end
    end
     end
    p=p+2;
    q=q+2;
 end


Kdam(1,1)=1E15;
    Kdam(2,2)=1E15;
%*******************************************************
[evecdam,evaldam]=eig(Kdam,M);

for i=1:nelm
    k1=i*2-1;
   Vdam(i,1)=evecdam(k1,1);
   Vdam(i,2)=evecdam(k1,2);
   Vdam(i,3)=evecdam(k1,3);
   Vdam(i,4)=evecdam(k1,4);
   Vdam(i,5)=evecdam(k1,5);

end
for i=1:ndof;
    evaldam(i,i)=sqrt(evaldam(i,i));
    fhzdam(i,i)= evaldam(i,i)/(2*pi);
end

Vall(nelm,10)=0;
Vall(1:nelm,1:5)=V;
```

```
Vall(1:nelm,6:10)=Vdam;

%Plotting of mode shapes
Height=[0;5;10;15;20;25;30;35;40;45;50;55;60;65;70;75;80
]
%for i=1:3
   %subplot(1,3,i)
   %plot([0; V(:,i)],Height,'r--o', 'linewidth',2,
'markersize',5,
'markeredgecolor','r','markerfacecolor','r');
   %hold on
   %plot([0; Vdam(:,i)],Height,'g--o', 'linewidth',2,
'markersize',5,
'markeredgecolor','g','markerfacecolor','g');
   %hold off
   %ylabel('Height of the Structure (m)',
'FontName','TimesNewRoman','fontweight','bold','fontangl
e',...
   %    'italic','fontsize',16,'color','k');
   % xlabel('Magnitude',
'FontName','TimesNewRoman','fontweight','bold','fontangl
e',...
%'italic','fontsize',16,'color','k')
    %title(['Mode Shape',num2str(i)],'Fontsize',18)
%end

%*****************************************************
%DAMAGED ith modal stiffness, Ki of the arbitrary
structure
Kidam(1,ndof)=0;
for i=1:ndof
    Kidam(1,i)=evecdam(:,i)'* K *evecdam(:,i);
end

%*****************************************************
%DAMAGE Localization Indicator Z
Ztop(ndof,nelm)=0.0;
Zk(nelm,ndof)=0.0;

for ii=1:nelm
    for jj=1:3
        for kk=1:nelm

Zk(kk,jj)=evecdam(:,jj)'*Kjo(:,:,kk)*evecdam(:,jj);
```

```
            Zk=sum(Zk,1);

Ztop(jj,ii)=((evecdam(:,jj)'*Kjo(:,:,ii)*evecdam(:,jj)+Z
k(1,jj))*Ki(1,jj));
            Ztop=sum(Ztop,1);

        end
    end
end

Zbot(ndof,nelm)=0.0;
Zy(nelm,ndof)=0.0;

for ii=1:nelm
    for jj=1:3
        for kk=1:nelm

Zy(kk,jj)=evec(:,jj)'*Kjo(:,:,kk)*evec(:,jj);
            Zy=sum(Zy,1);

Zbot(jj,ii)=((evec(:,jj)'*Kjo(:,:,ii)*evec(:,jj)+Zy(1,jj
))*Kidam(1,jj));
            Zbot=sum(Zbot,1);
        end
    end
end

Z(1,nelm)=0;
for i=1:nelm
    Z(1,i)=Ztop(1,i)/Zbot(1,i);
    alpha(1,i)=1/Z(1,i)-1;
end
Zmean=sum(Z,2)/nelm;
Zstand=std(Z);
Zj(1,nelm)=0;
for i=1:nelm
    Zj(1,i)=(Z(1,i)-Zmean)/Zstand;
end

%Statistical Hypothesis
H(1,nelm)=0;
for i=1:nelm
if Zj(i)>2
    H(1,i)=1;
```

```
else
    H(1,i)=0;
end
end

bar(Zj)
xlabel('Member Number','fontsize',16,'color','k')
ylabel('INDICATOR Z','fontsize',16,'color','k')
```

Frequency Based Damage Detection

```
clc
clear all

nelm=16;
ndof= 2*nelm+2 ;
M(ndof,ndof)=0.0;
K(ndof,ndof)=0.0;

roh=7800;
A=0.124;
E=2E11; %(N/mm^2)
 I=0.06; %(mm^4)
 l=80/nelm;
 Ke(1,1)= (E*I/l^3)*12;
 Ke(1,2)= (E*I/l^3)*6*l;
 Ke(1,3)= (E*I/l^3)*(-12);
 Ke(1,4)= (E*I/l^3)*6*l;
 Ke(2,2)= (E*I/l^3)*4*l^2;
 Ke(2,3)= (E*I/l^3)*(-6*l);
 Ke(2,4)= (E*I/l^3)*(2*l^2);
 Ke(3,3)= (E*I/l^3)*12;
 Ke(3,4)= (E*I/l^3)*(-6*l);
 Ke(4,4)= (E*I/l^3)*(4*l^2);
 Me= (roh*A*l/420)*[156 22*l 54 -13*l; 22*l 4*l^2 13*l -
3*l^2; 54 13*l 156 -22*l; -13*l -3*l^2 -22*l 4*l^2] ;
 for i=1:4
     for j=1:4
         Ke(j,i)= Ke(i,j);
     end
 end
 p=0;
 q=0;
 for ne=1:nelm
    for ii=1:4
```

```
        for jj=1:4
            M(p+ii,q+jj)=M(p+ii,q+jj)+ Me(ii,jj);
            K(p+ii,q+jj)=K(p+ii,q+jj)+ Ke(ii,jj);
         end
    end
    p=p+2;
    q=q+2;
 end

    K(1,1)=1E15;
    K(2,2)=1E15;
%*******************************
% ei=eig(K,M);
[evec,eval]=eig(K,M);


for i=1:ndof;
    eval(i,i)=sqrt(eval(i,i));
    fhz(i,i)= eval(i,i)/(2*pi);
end
%Consider only Vertical DOF

for i=1:nelm
    k1=i*2-1;
   V(i,1)=evec(k1,1);
   V(i,2)=evec(k1,2);
   V(i,3)=evec(k1,3);
   V(i,4)=evec(k1,4);
   V(i,5)=evec(k1,5);

end



%*****************************************************
%The ith modal stiffness, Ki of the arbitrary structure
Ki(1,ndof)=0;
for i=1:ndof
    Ki(1,i)=evec(:,i)'* K * evec(:,i);
end

%*****************************************************
```

```
%Defining Kj the contribution of the jth member to the
system stiffness
%matrix
Kj(ndof,ndof,nelm)=0.0;
a=0;
 b=0;
 for ne=1:nelm
    for ii=1:4
        for jj=1:4
            Kj(a+ii,b+jj,ne)=Kj(a+ii,b+jj,ne)+
Ke(ii,jj);
         end
    end
    a=a+2;
    b=b+2;
 end
Kj(1,1,1)=1E15;
  Kj(2,2,1)=1E15;

%*******************************************************
%The contribution of the jth member to the ith modal
stiffness Kij
Kij(nelm,ndof)=0.0;
for i=1:nelm
    for j=1:ndof
    Kij(i,j)=evec(:,j)'* Kj(:,:,i) * evec(:,j);
    end
end

%Fij, the fraction of modal energy(sensitivity) for the
ith mode that is
%concentrated in jth element
Fij(nelm,ndof)=0;
for i=1:ndof
   for  j=1:nelm
    Fij(j,i)=Kij(j,i)/Ki(i);
   end
end

%*******************************************************
%Defining Young's Modulus (Ej) of the system, and
solving Kjo involving the
%geometric quantities of the system
```

```
Kjo(ndof,ndof,nelm)=0.0;
a=0;
  b=0;
for ne=1:nelm
    for ii=1:4
        for jj=1:4
           Kjo(a+ii,b+jj,ne)=Kj(a+ii,b+jj,ne)/E;
        end
    end
    a=a+2;
    b=b+2;
end

%DAMAGED scenorio of the system
Kdam(ndof,ndof)=0.0;
p=0;
   q=0;
D=12;
 for ne=1:nelm
     if ne == D
       for ii=1:4
        for jj=1:4
          Kdam(p+ii,q+jj)=Kdam(p+ii,q+jj)+
Ke(ii,jj)*0.9;
        end
       end
      else
    for ii=1:4
        for jj=1:4
           Kdam(p+ii,q+jj)=Kdam(p+ii,q+jj)+ Ke(ii,jj);
         end
    end
     end
    p=p+2;
    q=q+2;
 end


Kdam(1,1)=1E15;
    Kdam(2,2)=1E15;
%*****************************************************
[evecdam,evaldam]=eig(Kdam,M);
```

```
for i=1:nelm
    k1=i*2-1;
   Vdam(i,1)=evecdam(k1,1);
   Vdam(i,2)=evecdam(k1,2);
   Vdam(i,3)=evecdam(k1,3);
   Vdam(i,4)=evecdam(k1,4);
   Vdam(i,5)=evecdam(k1,5);

end
for i=1:ndof;
    evaldam(i,i)=sqrt(evaldam(i,i));
    fhzdam(i,i)= evaldam(i,i)/(2*pi);
end


%*****************************************************
%DAMAGED ith modal stiffness, Ki of the arbitrary
structure
Kidam(1,ndof)=0;
for i=1:ndof
    Kidam(1,i)=evecdam(:,i)'* K *evecdam(:,i);
end
m=3; n=4;
%Calculating L.H.S
Zm=(evaldam(m,m)-eval(m,m))/eval(m,m);
l=0;
Za(n,n)=0;
for i=1:n
    Za(i,i)=(evaldam(i,i)-eval(i,i))/eval(i,i);
end
Zk(1,n)=0;
for i=1:n
    Zk(1,i)=Za(i,i);
end
Zk=sum(Zk,2);

%Calculating R.H.S
Fmq(nelm,1)=0;
for i=1:nelm
    Fmq(i,1)=Fij(i,3);
end
Fka(nelm,n)=0;
for i=1:n
    for j=1:nelm
```

```
    Fka(j,i)=Fij(j,i);
    end
end
Fkq=sum(Fka,2);

ej(nelm,1)=0;
for i=1:nelm
    ej(i,1)=Zm/Zk-(Fmq(i,1)/Fkq(i,1));
end

for i=1:nelm
    ej(i,1)=sqrt(ej(i,1)^2)
end


bar(ej)
xlabel('Member Number','fontsize',16,'color','k')
ylabel('INDICATOR Z','fontsize',16,'color','k')
```